THE JOURNAL OF PHYSICAL CHEMISTRY B

ARTICLE

pubs.acs.org/JPCB

Influence of Hydrodynamics on Cluster Formation in Colloid−Polymer Mixtures

Jonathan K. Whitmer[†] and Erik Luijten*[,‡]

[†]Department of Materials Science and Engineering and Department of Physics, University of Illinois at Urbana−Champaign, Urbana, Illinois 61801, United States

[‡]Department of Materials Science and Engineering and Department of Engineering Sciences and Applied Mathematics, Northwestern University, Evanston, Illinois 60208, United States

ABSTRACT:

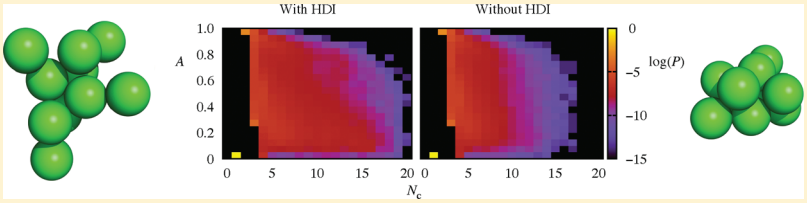

We investigate the role of hydrodynamic interactions in the formation of clusters of attractive colloids by means of computer simulations. In simulations employing the multiparticle collision dynamics scheme to represent hydrodynamics, larger and, to a lesser extent, more elongated transient clusters are formed than in simulations merely employing Langevin dynamics. As these clusters constitute the precursors to a colloidal gel, their shape affects the structure of the gel as well as the threshold concentration and colloidal attraction strength at which gelation occurs. Our findings support recent observations regarding the effect of hydrodynamics on colloidal gel formation.

INTRODUCTION

Gelation in colloidal suspensions is the aggregation of attractive particles into a network structure exhibiting mechanical stability. This phenomenon is relevant in a broad range of settings, including biological systems and industrial applications, where it can be either undesirable, such as in the manufacturing of stable liquid suspensions or colloidal crystals,[1,2] or useful, such as in the modification of the texture of food products[3] or cosmetics.[4] Control over the formation of a gel, which is an intrinsic nonequilibrium process, requires understanding of the dynamical pathways leading to colloidal aggregates.

Recently, computer simulations have shown that the presence of hydrodynamic interactions (HDI) has a strong influence on this aggregation process.[5] Specifically, suspensions of attractive colloids that interact hydrodynamically form stable, percolating structures at smaller attraction strengths than systems in which the colloids experience only Brownian motion. It is suggested[5,6] that this difference results from "squeezing" forces induced between colloidal aggregates. This hydrodynamic effect arises from solvent displaced by approaching clusters; the character of the generated flow rotates the aggregates, causing them to assemble into elongated structures, which in turn promotes percolation at lower volume fractions. Computer simulations indeed provide a suitable testing ground for studying the conditions under which this behavior is important, because they permit direct access to microscopic details and offer the freedom to tune various system parameters. However, because of technical limitations, only relatively few simulations of aggregating colloidal suspensions have simultaneously incorporated hydrodynamic and Brownian effects. It is the purpose of this work to address this and to further explore the observations of ref 5, with a particular emphasis on the formation of small colloidal clusters in the presence of hydrodynamic interactions.

Much early understanding of colloidal aggregation was obtained in the diffusion-limited cluster-aggregation (DLCA) limit, where clusters are formed as particles diffuse, fusing irreversibly when they contact other particles or aggregates.[7,8] If the interparticle attractions are less strong, structures form that subsequently relax into dense-packed clusters.[9] In this case, percolating gels arise through a process of assembly of particles into clusters, and of clusters into the final aggregate. Consequently, the shape of these clusters crucially affects the structure of the final gel, as well as the packing fraction of particles required for the system to become mechanically stable.

The shape of small clusters of short-range attractive colloids in equilibrium can be understood from simple geometric packing rules.[10,11] In the presence of long-range repulsions, such clusters can form a stable phase, rather than a gel state.[12] However, in the context of colloidal gels, we are interested in states which become arrested before reaching their global free-energy minimum. The assembly of particles is influenced simultaneously by the strength

Special Issue: Clusters in Complex Fluids

Received: November 30, 2010
Revised: March 31, 2011
Published: May 16, 2011

of the interactions and the shape of the constituents. At large attraction strengths, the DLCA limit is approached and gelation into an open, low-density structure occurs. Likewise, aggregates with low volume fraction arise in suspensions of particles with large aspect ratio, which can form space-filling structures at much lower density than their spherical counterparts.[13,14] A related effect occurs in colloidal systems that favor the formation of elongated, rod-like structures. These systems form more open, branched, percolating networks[15,16] than systems that favor spherical cluster formation.[12]

In two-dimensional simulations, it has been shown that hydrodynamic interactions can lead to the formation of colloidal structures that are more elongated than when the solvent is assumed to only affect the single-particle drag coefficients.[17,18] If these *transient* structures, which do not constitute global minima of the cluster potential-energy landscape, are sufficiently long-lived, we can reason that they would act and assemble as rods do, thus permitting gels to form at lower attraction strengths and volume fractions than one would otherwise expect. Recent simulation studies which examine this effect in three dimensions[5,18] seem to offer conflicting evidence —ref 18 states that hydrodynamics only minimally affects the final structure of a colloidal gel in three dimensions, while ref 5 states that gels will form at lower attraction strength with hydrodynamic interactions present than without. Here, we attempt to systematically address how the strength and range of colloidal interactions can influence the transient clusters that form, to better understand the rule of hydrodynamics in gelation. We do this by performing simulations with and without hydrodynamics, varying attraction strength and range. Instead of focusing on colloidal gels, we are interested in the hydrodynamic influence on the conformations of small ($N \leq 20$) particle clusters and demonstrate that already these precursors to colloidal gels are susceptible to the presence of hydrodynamic interactions, adopting shapes that ultimately affect the conditions under which the formation of a space-spanning network occurs. As our interest is in the transient cluster formation, these simulations are inherently nonequilibrium.

SIMULATION METHOD

We utilize a hybrid molecular dynamics (MD) and multiparticle collision dynamics (MPC)[19,20] scheme to study colloidal suspensions. Attractive interactions are introduced between colloidal particles through a modified Asakura−Oosawa−Vrij (AOV) potential.[21,22] This potential models the depletion interactions between colloids induced by weakly interacting, nonadsorbing polymers. The modification is required to provide a repulsive core (representing excluded-volume interactions) that can be integrated via molecular dynamics. The simulations of ref 5 also use this potential, although with a different modification than used here. Of chief interest is the limit in which the attraction is short-ranged. In this limit, it has recently been shown[23] through a combination of computer simulation and experiment that the *shape* (i.e., functional dependence on particle separation) of the interaction is unimportant for determining the onset of gelation in the system—this is determined solely by the second virial coefficient. However, the range over which colloidal particles interact is likely important when considering how attraction and hydrodynamic forces influence their rearrangement during bonding. The range of attraction in the AOV model is determined by $\zeta \equiv 2R_g/\sigma_{cc}$, the radius of gyration R_g of the polymer normalized by the colloidal radius $\sigma_{cc}/2$. The strength of the attraction is controlled by ζ and by the polymer concentration ϕ_p.

The precise form of the potential follows the choices of ref 24. We combine an AOV potential

$$\beta U_{AOV}(r) = -\phi_p\left(\frac{1+\zeta}{\zeta}\right)^3\left[1-\frac{3r/\sigma_{cc}}{2(1+\zeta)}+\frac{1}{2}\left(\frac{r/\sigma_{cc}}{1+\zeta}\right)^3\right] \quad \text{for} \quad 1 < r/\sigma_{cc} < (1+\zeta) \tag{1}$$

with a $1/r^{36}$ soft-sphere potential smoothly defining the particle cores and a quadratic minimum[25] that ensures that the position of the attractive well is independent of the depletion strength. As usual, $\beta = 1/(k_BT)$, with T the absolute temperature and k_B Boltzmann's constant. To ensure that the entire potential is smooth at the boundary of the attractive region $[r = (1+\zeta)\sigma_{cc}]$, we supplement this potential with a $1/r^{18}$ term. Defining $\alpha_2 = (1+\zeta)\sigma_{cc}$, we write the resulting pair interaction as

$$\beta U(r) = \beta U_{ss}(r) + \beta U_{att}(r) \tag{2}$$

where the soft-sphere contribution is given by

$$\beta U_{ss}(r) = \alpha_1\left(\frac{1}{r^{36}}-\frac{2}{\alpha_2^{18}r^{18}}+\frac{1}{\alpha_2^{36}}\right) \quad \text{if} \quad r \leq \alpha_2 \tag{3}$$

and the modified depletion interaction by

$$\beta U_{att}(r) = \begin{cases} B(r-\sigma_{cc})^2 + C & \text{if } 0 < r < (1+\alpha_3\zeta)\sigma_{cc} \\ \beta U_{AOV}(r) & \text{if } (1+\alpha_3\zeta)\sigma_{cc} \leq r < \alpha_2 \end{cases} \tag{4}$$

The crossover point is set by the parameter α_3 (equal to 0.1 for the simulations presented here). The constants B and C then follow from continuity of both βU_{att} and its first derivative at $r = (1+\alpha_3\zeta)\sigma_{cc}$

$$B = \frac{3\phi_p}{4\alpha_3\zeta^4\sigma_{cc}^2}((1+\zeta)^2-(1+\alpha_3\zeta)^2) \tag{5}$$

$$C = \beta U_{AOV}(r = \sigma_{cc}(1+\alpha_3\zeta)) - B(\alpha_3\zeta\sigma_{cc})^2 \tag{6}$$

The colloid size is set to $\sigma_{cc} = 4.3a_0$ (where a_0 is a length scale pertaining to the hydrodynamics simulations, introduced below), and the parameter α_1 (eq 3) is set to σ_{cc}^{36}. In this study, we employ three different sets of potential-energy parameters, which are summarized in Table 1. For comparison and illustration, the simulation potential (eq 2) is plotted for one of these cases, together with the corresponding AOV potential (eq 1) in Figure 1. The larger value of the range parameter ζ (first two parameter sets) is chosen to connect to the simulations presented in ref 5.

To investigate the role of hydrodynamic interactions, we perform two types of simulations with this potential. The first type uses an implicit solvent represented by Langevin dynamics (i.e., a conventional molecular dynamics simulation *without* hydrodynamic interactions), whereas the second type uses an explicit fluid modeled through MPC to include hydrodynamic interactions. In this method, momentum exchange between fluid elements takes place through random collisions within subcells of the system. For a detailed description and a review of various applications of the method, see refs 26 and 27. There exist several variants of MPC, distinguished by the mechanism used for momentum exchange between fluid elements. Here, we utilize the stochastic rotation dynamics variant[19,20] with a rotation angle

Table 1. Combinations of Potential-Energy Parameters Used for the Simulations[a]

βU_{AOV}	ζ	ϕ_p	βU_{actual}
−3.00	0.347	0.560	−1.71
−6.00	0.347	1.120	−4.40
−4.71	0.072	0.216	−3.81

[a] βU_{actual} refers to the actual depth of the potential at contact.

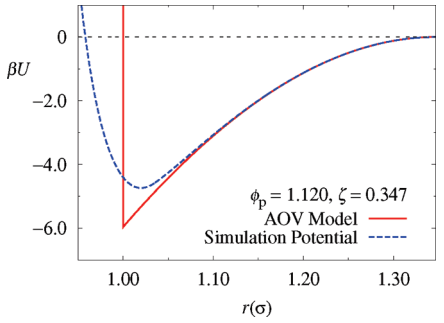

Figure 1. Modified depletion potential (eqs 2−4) for one of the three parameter sets employed in the present work (cf. Table 1), along with the corresponding AOV potential (eq 1) for hard-sphere colloids.

of $\pi/2$. Since the MPC simulations are computationally demanding, we limit ourselves to $N = 20$ colloids placed in a cubic, periodically replicated system of linear dimension $L = 32a_0$, where a_0 is the linear size of the collision cell. For consistency, the Langevin simulations use the same number of colloids and the same system size. Although the total number of colloids is relatively small, it is sufficient to study the early stages of cluster formation and the effect of hydrodynamics. Also, the system is large enough to minimize finite-size effects. As in previous MPC simulations,[28,29] we set the fluid density to five particles per collision cell (160488 fluid particles total). The fluid particles have mass m_f and the time between collision steps is set to $0.1a_0/(k_BT/m_f)^{1/2}$. The colloids have mass $125m_f$. For convenience, all units are reduced such that $a_0 = k_BT = m_f = 1$.[28] This sets the natural MPC time scale $t_0 = a_0/(k_BT/m_f)^{1/2} = 1$.

To allow a direct mapping of the time scales in the simulations with and without hydrodynamic interactions, the friction coefficient in the Langevin simulations is set to match that measured for isolated colloids in the MPC simulations. In the latter, fluid−colloid interactions are implemented through purely repulsive central forces originating from a shifted-truncated Lennard-Jones interaction with strength parameter $2.5k_BT$ and range parameter equal to $a = 2a_0$. This type of colloid−fluid interactions yields slip boundary conditions at the colloid surface. The colloid−colloid interaction diameter $\sigma_{cc} = 4.3a_0 = 2.15a$ is deliberately chosen slightly larger than $2a$ to eliminate spurious depletion forces that result from the use of an explicit solvent.[28] The resulting colloidal volume fraction is $\phi_c = 0.0254$, but we note that its precise value is far less relevant for cluster formation than for actual gelation.

To properly represent the squeezing forces between colloids, the fluid must be incompressible.[5] It should be noted that, although the fluid in our simulations is compressible, it is not free-draining; thus, many of the effects of squeezing flow related to displacement of fluid should be well represented. Furthermore, the MPC fluid will behave as an incompressible fluid provided the Mach number $Ma = v_c/c_s$ is small, where v_c denotes the characteristic velocity of the colloidal particles and c_s is the speed of sound.

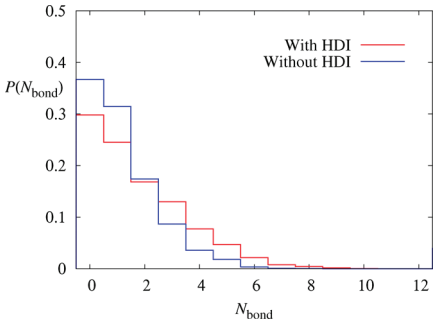

Figure 2. Bond number probability distribution for colloids with attraction strength $-3k_BT$. "HDI" refers to hydrodynamic interactions.

Lastly, we note that the small range of the colloidal attractions necessitates the use of a small time step to properly integrate the equations of motion. In our case, we choose an integration time step $\Delta t_{MD} = 0.005t_0$ with fluid−fluid interactions computed via MPC every $20\Delta t_{MD}$. This leads to fairly slow evolution even for systems with small numbers of colloids; the simulations for this paper required 384 CPU days to complete.

CLUSTER ANALYSIS

We focus on simulations with a depletion strength of $U_{AOV} = -3k_BT$ (cf. Table 1), as this is sufficiently weak to permit significant rearrangements even after colloidal clusters have formed. Thus, we expect this case to be the most susceptible to hydrodynamic effects; it is also the choice for which gelation is first observed in ref 5. Starting from random, homogeneous distributions of colloids, we perform 96 simulations, each over 7.5×10^6 time steps, which corresponds to $176\tau_D$, where $\tau_D = a^2/D_{self}$ is the time required for a free (dilute) particle to diffuse one colloidal radius. We monitor each system from $t = 88\tau_D$ to $t = 176\tau_D$ and average over the 96 independent runs.

As a first measure of the clusters that form in these simulations, we consider the coordination number, where a bond is defined between each pair of colloids that have a center-to-center distance less than $(1 + \zeta)\sigma_{cc}$. As shown in Figure 2, particles in systems with MPC solvent have a larger average number of neighbors than particles in systems simulated with an implicit solvent. Although one may expect elongated clusters to have a smaller number of neighbors per particle than tightly packed, sphere-like clusters, care must be taken when applying this logic to small clusters and when comparing clusters of different sizes.

Thus, to quantify the structure of these clusters in further detail, we examine the radius of gyration tensor.[30] The trace of this tensor yields the squared radius of gyration, R_g^2, while its eigenvalues λ_i $(i = 1, 2, 3)$ yield the asphericity[31]

$$A = \frac{1}{2}\frac{(\lambda_1-\lambda_2)^2+(\lambda_2-\lambda_3)^2+(\lambda_3-\lambda_1)^2}{(\lambda_1+\lambda_2+\lambda_3)^2} \qquad (7)$$

This measure $(A \in [0,1])$ is commonly used to characterize the geometry of random walks and polymers.[32] It is equal to zero for perfectly spherical clusters and equal to 1 for perfectly linear clusters, so that larger asphericities imply more elongated particle conformations. The left-hand panel of Figure 3 illustrates the mutual distribution of asphericity and cluster size in simulations that include hydrodynamic interactions, to be contrasted with the right-hand panel showing the same distribution in the

absence of hydrodynamics. In both graphs, black pixels indicate that a conformation is not observed in simulation. Interestingly, the simulations with hydrodynamic interactions show a tendency toward the formation of larger clusters, which in turn explains the shifted bond-number distribution of Figure 2. In addition, a more subtle feature is apparent in these simulations, namely, a bimodal distribution in the asphericity for medium-sized clusters, with peaks corresponding to near-spherical and nearly rod-like structures—an effect more pronounced with HDI than without. This behavior can be elucidated by examining the marginal distributions of A along slices of constant N_c, shown in Figure 4a,b. Indeed, for clusters of size $N_c = 10$, a secondary peak near $A \approx 0.8$ is found for the MPC simulations (Figure 4a), indicating that there is a "p—ocket of stability" for larger, elongated clusters. Examples of $N_c = 10$ clusters observed in simulations with HDI are shown in panels c and d of Figure 4.

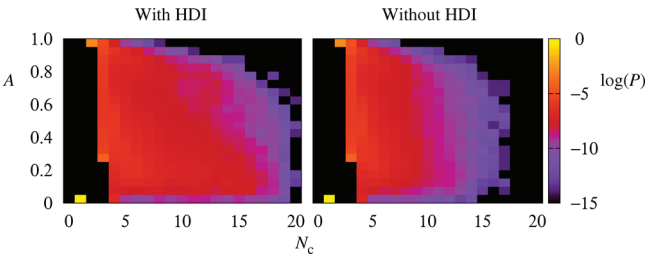

Figure 3. Probability density map showing the mutual probability distribution of asphericity A and cluster size N_c for simulations at $U_{AOV} = -3k_BT$. The left-hand panel results from simulations including hydrodynamic interactions, whereas the right-hand panel pertains to simulations in which hydrodynamic interactions are omitted. Hydrodynamic effects lead to a pronounced enhancement of the formation of larger clusters.

As a last measure of the cluster structure, we plot in Figure 5 the cluster size probability, which further confirms the tendency of simulations involving hydrodynamic interactions to form larger clusters. At this attraction strength, clusters are constantly forming and breaking apart into clusters of different sizes. This also explains the bimodal nature of the asphericity distribution $P(A)$. Under the influence of hydrodynamics, small clusters join to form transient, elongated structures that subsequently break up again into small, more spherical clusters.

We further examine the same system at a larger attraction strength of $-6k_BT$. As expected, the bond distribution shifts to larger bond numbers per colloid. However, there no longer is a significant difference between simulations with and without hydrodynamics. This is confirmed in Figure 6, which shows that the probability distribution is very strongly skewed toward the largest clusters. Smaller cluster states exhibit a bimodality similar to the $-3k_BT$ case, but these are all low-probability states; the final state of many of the runs consists of a single $N_c = 20$ cluster. As illustrated by

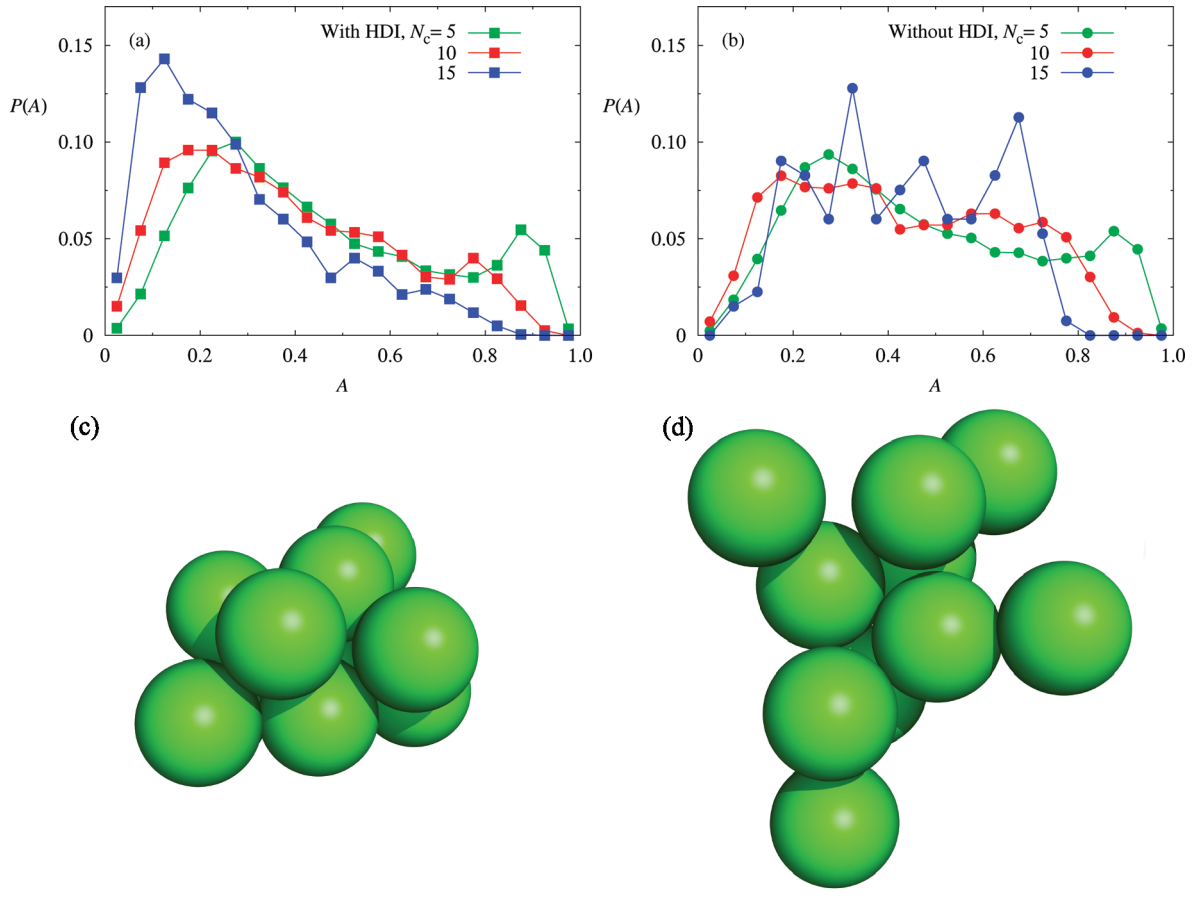

Figure 4. Marginal distributions of the cluster asphericity A, obtained from Figure 3 for slices of constant N_c = 5, 10, and 15. Under the influence of hydrodynamics (panel a), the distribution for $N_c = 10$ shows a secondary peak for larger $A \approx 0.8$, corresponding to the formation of elongated clusters. The jagged appearance of $P(A)$ in panel b originates from poor statistics; at this attraction strength, the formation of larger clusters is very rare in the absence of hydrodynamic effects. Panels c and d show observed $N_c = 10$ configurations corresponding to the two peaks in the distribution of panel a, with asphericities of 0.07 and 0.81, respectively.

dx.doi.org/10.1021/jp111388m |J. Phys. Chem. B 2011, 115, 7294–7300

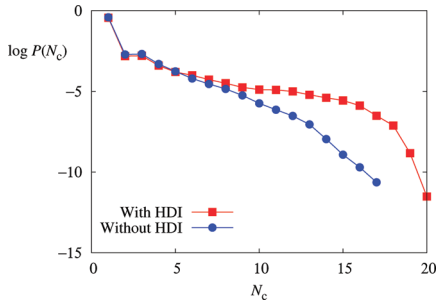

Figure 5. Probability distribution for a given cluster to have N_c constituents in simulations with colloidal attraction strength $U_{AOV} = -3k_BT$. This highlights how hydrodynamic effects promote cluster formation.

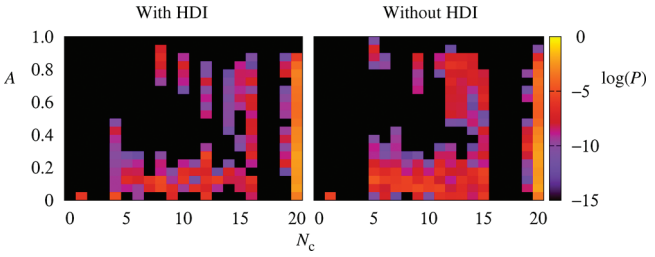

Figure 6. Probability density map showing the mutual probability distribution of asphericity A and cluster size N_c for simulations at $U_{AOV} = -6k_BT$. The left panel results from simulations including hydrodynamic interactions, whereas the right panel pertains to simulations in which hydrodynamic interactions are omitted. At this large attraction strength, both types of simulations yield predominantly large clusters.

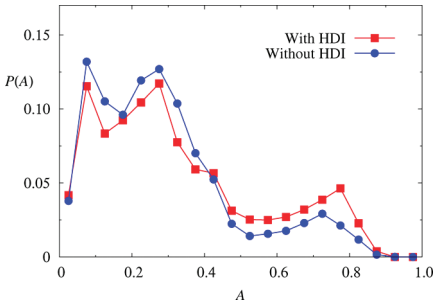

Figure 7. Marginal probability distribution of the asphericity A of clusters containing 20 colloids, at attraction strength $U_{AOV} = -6k_BT$. Unlike the situation for twice weaker attraction strength (Figure 4), there is no significant influence of hydrodynamic effects.

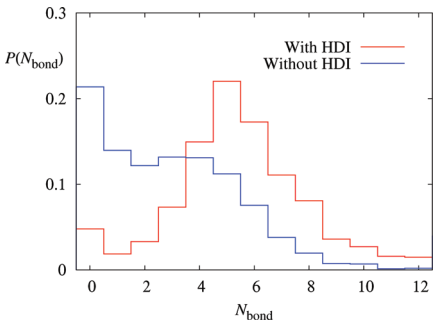

Figure 8. Bond number probability distribution for a system with a depletion attraction with a range that is 5 times smaller than that for the system depicted in Figure 2. The strength of the attraction ($-4.71k_BT$) is chosen such that the second virial coefficient of this system matches that of the $-3k_BT$ potential used in Figure 2.

Figure 7, there is no strong difference in asphericity between such clusters generated with or without hydrodynamics.

It is conceivable that the range of the attractive interactions influences the cluster conformations. To investigate this, we reduce the depletant size by almost a factor of 5 to $\zeta = 0.072$. This matches our previous simulations for colloidal sedimentation,[24] as well as experiments on colloidal gels.[33] Following the recent finding[23] (based in turn upon an earlier computational observation[34]) that the particle concentration required for gelation can be universally characterized through the second virial coefficient, we set $U_{AOV} = -4.71k_BT$. Thus, this system is predicted to exhibit the same type of clustering behavior as the suspension with $U_{AOV} = -3k_BT$, despite the much shorter attraction range. However, examination of Figure 8 shows a bond number distribution markedly different from that in Figure 2, with the hydrodynamic simulations strongly skewed toward greater connectivity. Here, the neighbor distribution is sufficiently shifted to create a peak at around 6 neighbors per particle.

The details of this connectivity are best captured through the marginal distributions for A at each N_c (Figure 9). Here, we note again the bimodal nature of the asphericity distribution for simulations with HDI at large cluster sizes. The absence of this bimodality for $N_c = 10$ in Figure 9a is not significant, as such clusters have a very low probability in simulations with HDI, see Figure 10. Indeed, the overall cluster size distribution shows considerable separation between simulations with and without HDI.

DISCUSSION

The cluster analysis in the preceding section demonstrates that, within the range of variation of our simulations, the types of clusters formed with and without hydrodynamic interactions differ, with hydrodynamic simulations exhibiting a tendency to form larger and sometimes more elongated transient clusters. This result supports the findings of ref 5, where hydrodynamics were found to promote gelation, especially at moderate attraction strengths. At larger attraction strengths, we observe no strong difference in cluster size and shape distribution for simulations with and without hydrodynamic interactions. This is in agreement with the expectation that ultimately (i.e., when one approaches the DLCA limit) the attraction strength is the dominant determinant for the cluster shape and consequently for the connective geometry of the gel. We emphasize that the effects of hydrodynamics are best seen from the bimodal distributions for $N_c = 10$ in Figure 4a and for $N_c = 20$ in Figure 9a, while keeping in mind that the corresponding data for simulations *without* hydrodynamic interactions exhibit very poor statistics, since such clusters rarely form in these simulations (cf. Figure 3).

In the fluid particle dynamics (FPD) method used in ref 5, colloids are represented as "fluid" regions of very high viscosity. Since the fluid velocity field must be single-valued, colloids at contact experience strong lubrication and friction forces that are not present in the MPC method employed here. Whereas thermal fluctuations will allow colloidal aggregates to relax into structures of lower potential energy, the dynamics is significantly affected by the colloidal friction. Thus, it is well possible that the elongated clusters which in our simulations have a relatively transient nature are more long-lived in the FPD simulations. Another difference between our

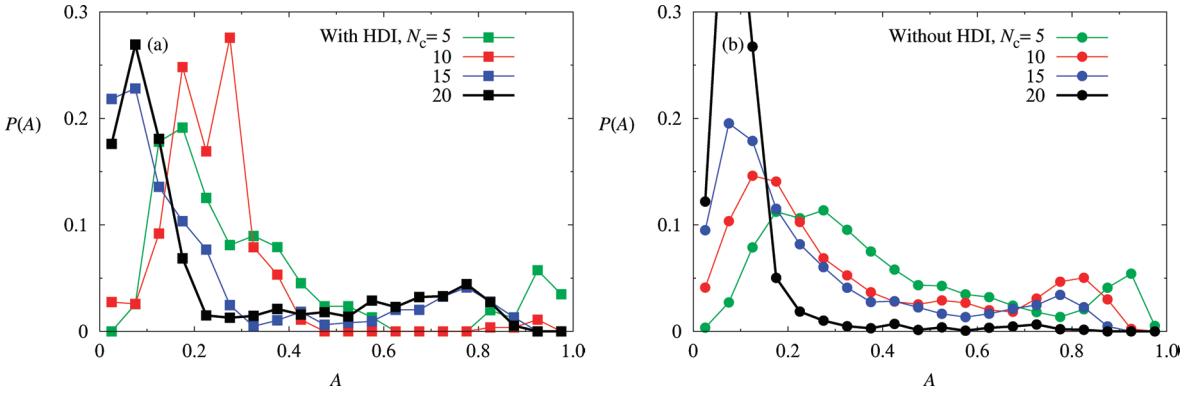

Figure 9. Marginal probability distributions for the asphericity A at constant N_c = 5, 10, 15, and 20 in simulations of colloids with attraction strength $-4.71k_BT$ and range $\zeta = 0.072$. Observe the secondary peak near $A \approx 0.75$ for the $N_c = 20$ data in the presence of hydrodynamic interactions (panel a).

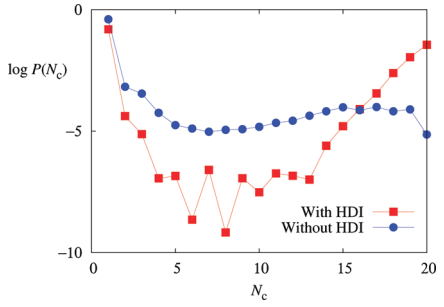

Figure 10. Probability distribution for a given cluster to have N_c constituents in simulations with colloidal attraction strength $U_{AOV} = -4.71k_BT$ and attraction range $\zeta = 0.072$. Comparison to the corresponding graph for a system with identical second virial coefficient but significantly larger attraction range $\zeta = 0.347$ and correspondingly weaker attraction $U_{AOV} = -3k_BT$ (Figure 5) shows that stronger, more short-ranged interactions result in larger clusters. Nevertheless, the influence of hydrodynamic effects is still clearly detectable, resulting in even larger clusters than in the presence of diffusive motion alone.

simulations and the FPD-based calculations is that we impose slip boundary conditions for the fluid at the colloidal surface, whereas the FPD method employs stick boundary conditions. To investigate the role of this choice, we have repeated the calculations for our first parameter set ($U_{AOV} = -3k_BT$, $\zeta = 0.347$) with stick boundary conditions.[29] We found that this has only a small effect on the cluster size and shape distribution.

In experiments, frictional contacts will also retard the relaxation of colloidal aggregates (cf. the influence of friction on the random loose packing fraction of spheres[35,36]), thus increasing the lifetime of elongated clusters and permitting them to persist during the aggregation of clusters into a gel. Lastly, a factor that we have not pursued here is the role of solvent viscosity. The strength of the squeezing forces is proportional to the viscosity of the suspension and the approach velocity of the two surfaces,[37] and thus we anticipate it to affect the cluster formation process. Corresponding examinations are currently underway.

Our findings for $U_{AOV} = -3k_BT$ and $U_{AOV} = -6k_BT$ may also shed light upon the apparent contradiction between refs 18 and 5. In the former study, colloidal aggregation is observed upon a quench to effectively zero temperature (i.e., without taking into account Brownian motion), and it is explicitly stated that a quench to a finite temperature would not alter the findings.[18] However, such a deep quench implies very strong interactions—one effectively reaches the DLCA limit. Indeed, this is the very limit where hydrodynamic interactions are no longer relevant, cf. Figure 7. Conversely, significant hydrodynamic effects are observed in the current work and in ref 5 for much weaker colloidal attractions, and it seems plausible that the simulations of ref 18 would yield those effects as well for a less deep temperature quench.

It was shown earlier, through comparison of experiment (where hydrodynamic interactions are omnipresent) and simulations *without* hydrodynamic interactions, that for attractions with very short range the details of gelation only depend on the second virial coefficient and are not affected by the details of the interaction.[23] Our results for the cluster size distribution (cf. Figures 2 and 8) do not necessarily contradict this universality, since the system of Figure 2 presumably has an attraction range outside of the window of validity of this statement. However, our system with $U_{AOV} = -4.71k_BT$ and $\zeta = 0.072$ has a sufficiently short-ranged attraction. For this system, Figures 8 and 10 show a significant difference between simulations with and without hydrodynamic interactions. This seems difficult to reconcile with the observed agreement[23] between experiments with hydrodynamic interactions and simulations without hydrodynamic interactions.

In conclusion, we have performed simulations of suspensions of isotropically interacting colloids to identify the role of hydrodynamics in the cluster formation process. Our simulations demonstrate that, notably for moderate colloidal attraction strengths (i.e., near the gelation threshold) even for these precursors to the colloidal gel hydrodynamics is significant, thus promoting gelation through the preferential formation of larger, elongated clusters.

AUTHOR INFORMATION

Corresponding Author

*E-mail: luijten@northwestern.edu.

ACKNOWLEDGMENT

This material is based upon work supported by the National Science Foundation under Grant Nos. DMR-0346914 and DMR-1006430. The authors would like to thank Wei Qu for providing the code for analyzing the asphericity. We also acknowledge allocation of computing time on Northwestern University's Quest cluster.

REFERENCES

(1) Lee, W.; Chan, A.; Bevan, M. A.; Lewis, J. A.; Braun, P. V. *Langmuir* **2004**, *20*, 5262–5270.

(2) Martinez, C. J.; Liu, J.; Rhodes, S. K.; Luijten, E.; Weeks, E. R.; Lewis, J. A. *Langmuir* **2005**, *21*, 9978–9989.
(3) Allen, K. E.; Murray, B. S.; Dickinson, E. *Food Hydrocolloids* **2008**, *22*, 690–699.
(4) Gallegos, C.; Franco, J. M. *Curr. Opin. Colloid Interface Sci.* **1999**, *4*, 288–293.
(5) Furukawa, A.; Tanaka, H. *Phys. Rev. Lett.* **2010**, *104*, 245702.
(6) Tanaka, H.; Araki, T. *Chem. Eng. Sci.* **2006**, *61*, 2108–2141.
(7) Witten, T. A.; Sander, L. M. *Phys. Rev. Lett.* **1981**, *47*, 1400–1403.
(8) Poon, W. C. K.; Pirie, A. D.; Pusey, P. N. *Faraday Discuss.* **1995**, *101*, 65–76.
(9) Lu, P. J.; Conrad, J. C.; Wyss, H. M.; Schofield, A. B.; Weitz, D. A. *Phys. Rev. Lett.* **2006**, *96*, 028306.
(10) Arkus, N.; Manoharan, V. M.; Brenner, M. P. *Phys. Rev. Lett.* **2009**, *103*, 118303.
(11) Meng, G.; Arkus, N.; Brenner, M. P.; Manoharan, V. N. *Science* **2010**, *327*, 560–563. See also the theoretical supplementary information provided online.
(12) Sciortino, F.; Mossa, S.; Zaccarelli, E.; Tartaglia, P. *Phys. Rev. Lett.* **2004**, *93*, 055701.
(13) Philipse, A. P.; Wierenga, A. M. *Langmuir* **1998**, *14*, 49–54.
(14) Solomon, M. J.; Spicer, P. T. *Soft Matter* **2010**, *6*, 1391–1400.
(15) Sciortino, F.; Tartaglia, P.; Zaccarelli, E. *J. Phys. Chem. B* **2005**, *109*, 21942–21953.
(16) Campbell, A. I.; Anderson, V. J.; van Duijneveldt, J. S.; Bartlett, P. *Phys. Rev. Lett.* **2005**, *94*, 208301.
(17) Tanaka, H.; Araki, T. *Phys. Rev. Lett.* **2000**, *85*, 1338–1341.
(18) Yamamoto, R.; Kim, K.; Nakayama, Y.; Miyazaki, K.; Reichman, D. R. *J. Phys. Soc. Jpn.* **2008**, *77*, 084804.
(19) Malevanets, A.; Kapral, R. *J. Chem. Phys.* **1999**, *110*, 8605–8613.
(20) Malevanets, A.; Kapral, R. *J. Chem. Phys.* **2000**, *112*, 7260–7269.
(21) Asakura, S.; Oosawa, F. *J. Chem. Phys.* **1954**, *22*, 1255–1256.
(22) Vrij, A. *Pure Appl. Chem.* **1976**, *48*, 471–483.
(23) Lu, P. J.; Zaccarelli, E.; Ciulla, F.; Schofield, A. B.; Sciortino, F.; Weitz, D. A. *Nature* **2008**, *453*, 499–504.
(24) Whitmer, J. K.; Luijten, E. *J. Chem. Phys.* **2010**, *134*, 034510.
(25) Puertas, A. M.; Fuchs, M.; Cates, M. E. *Phys. Rev. E* **2003**, *67*, 031406.
(26) Kapral, R. *Adv. Chem. Phys.* **2008**, *140*, 89–146.
(27) Gompper, G.; Ihle, T.; Kroll, D. M.; Winkler, R. G. *Advanced Computer Simulation Approaches for Soft Matter Sciences III*; Advances in Polymer Science; Springer: Berlin, 2008; Vol. 221; pp 1−87.
(28) Padding, J. T.; Louis, A. A. *Phys. Rev. E* **2006**, *74*, 031402.
(29) Whitmer, J. K.; Luijten, E. *J. Phys.: Condens. Matter* **2010**, *22*, 104106.
(30) Šolc, K. *J. Chem. Phys.* **1971**, *55*, 335–344.
(31) Diehl, H. W.; Eisenriegler, E. *J. Phys. A* **1989**, *22*, L87–L91.
(32) Guo, L.; Luijten, E. *Macromolecules* **2003**, *36*, 8201–8204.
(33) Gao, Y.; Kilfoil, M. *J. Phys.: Condens. Matter* **2004**, *16*, S5191–S5202.
(34) Noro, M. G.; Frenkel, D. *J. Chem. Phys.* **2000**, *113*, 2941–2944.
(35) Martin, C. L.; Bordia, R. K. *Phys. Rev. E* **2008**, *77*, 031307.
(36) Farrell, G. R.; Martini, K. M.; Menon, N. *Soft Matter* **2010**, *6*, 2925–2930.
(37) Russel, W. B.; Saville, D. A.; Schowalter, W. R. *Colloidal Dispersions*; Cambridge University Press: Cambridge, U.K., 1989.